buildings

Article

Shear Behavior of FRP Connectors in Precast Sandwich Insulation Wall Panels

Dong Chen [1], Kuaikuai Li [1], Zhiyang Yuan [2], Baoquan Cheng [3,*] and Xing Kang [4]

[1] BIM Engineering Center of Anhui Province, Anhui Jianzhu University, Hefei 230601, China; chendong@ahjzu.edu.cn (D.C.); likuai@stu.ahjzu.edu.cn (K.L.)
[2] China Energy Construction City Investment Development Co. Ltd., Beijing 100020, China; 13865982971@163.com
[3] School of Civil Engineering, Central South University, Changsha 410083, China
[4] Anhui Jinggong Green Construction Group Co. Ltd., Hefei 230601, China; xing_kang@outlook.com
* Correspondence: curtis_ch@csu.edu.cn

Abstract: Glass fiber reinforced polymer (FRP) composite connectors used in precast sandwich insulation wall panels directly affect the safety of the wall. In practical applications, a precast concrete sandwich insulation wall panel is transported to the construction site for hoisting 3–5 days after steam curing, and its concrete strength typically reaches approximately 70% of the design strength (i.e., the concrete strength after natural curing for 14 days). This study investigated the natural curing of concrete for 14 days and analyzed the mechanical properties of FRP connectors with two different sections in terms of their failure mode, failure process, and load–displacement curves. Numerical analysis and finite element parametric analysis of the connectors were conducted based on experimental data. The average ultimate shear capacity of a single rectangular-section connector was 8.37 kN and that of the cross-section connector was 8.37 kN. The connectors exhibited a good shear resistance, and the rectangular-section connectors had better ductility than the cross-section connectors. The wall panel exhibited three types of failure modes: splicing failure of the fiber layer of the connector, fiber fracture in the anchorage of the connector, failure of the concrete of the anchorage, and mainly material damage of the connector itself. The error between the load simulation value and test value of a single connector was less than 10% of the numerical simulation error requirement, and the finite element simulation results were reliable. The results of the parametric simulation of the shear capacity showed that the distance between connectors, anchorage depth, and insulation layer thickness had a significant influence on the shear performance of concrete connectors.

Keywords: precast sandwich insulation wall panel; glass fiber reinforced polymer connector; failure morphology; bearing capacity; finite element simulation

Citation: Chen, D.; Li, K.; Yuan, Z.; Cheng, B.; Kang, X. Shear Behavior of FRP Connectors in Precast Sandwich Insulation Wall Panels. *Buildings* **2022**, *12*, 1095. https://doi.org/10.3390/buildings12081095

Academic Editor: Luca Pelà

Received: 29 June 2022
Accepted: 22 July 2022
Published: 26 July 2022

1. Introduction

In recent years, the problem of building energy consumption has been emphasized in many countries including in China. It is necessary to protect the environment, save energy, and reduce building energy consumption [1–3]. Precast sandwich insulation wall panels have excellent thermal insulation and are widely used in outer-wall envelope structures. Currently, most precast sandwich insulation wall panels use connectors to connect the inner leaf concrete, outer leaf concrete, and middle insulation layer of the composite wall panel. The connector has advantages such as low weight, good corrosion resistance, high-tensile-strength performance, and a thermal expansion coefficient close to that of concrete. Therefore, it is widely used in prefabricated sandwich insulation wall panels [4–7]. Since precast sandwich insulation wall panels are lifted and transported to the site for construction 3–5 days after steam curing, the concrete strength only reaches approximately 70% of the design strength [8,9] (i.e., the concrete strength after 14 days of natural curing). To improve the safety performance of precast sandwich insulation wall panels, scholars have conducted considerable research from the following aspects.

In construction, the connection effect of connectors directly affects the safety of prefabricated sandwich insulation wall panels. Connectors have been designed considering the types, materials, and layout, and their performance has been studied. For example, Salmon [10,11] applied the plane section assumption to analyze concrete sandwich insulation wall panels connected by ordinary steel bars. The panels exhibited poor insulation performance when the steel bar was used as the tie piece. Hence, this paper proposes a new material that can replace steel bars to improve the insulation performance of wall panels, namely fiber reinforced polymer (FRP). The entire theoretical framework of a sandwich panel has been formed on the basis of experiments, which have guiding significance for further research. Hamid [12] et al. conducted an experimental study on the durability of carbon fiber reinforced polymer (CFRP) and glass fiber reinforced polymer (GFRP) connectors in concrete sandwich insulation wall panels, and tests were conducted to analyze the influence of insulation layers of different materials on the shear properties of specimens. The results showed that expanded polystyrene board (EPS) has a higher shear resistance than extruded polystyrene board (XPS). Ekenel et al. [13] studied the mechanical properties of lattice FRP connectors, including their shear modulus, shear strength, and stiffness. The formulae derived from the above parameters produced results that were in good agreement with the experimental results, and the theoretical formulae have been adopted in relevant specifications. Portal et al. [14] used both GFRP plate connector and bar connector in composite wall panels, where the GFRP plate connector was anchored with steel bars. The wall panel could be combined, and the connector was pulled out. Chen [15] conducted a bending test on a composite wall plate with an FRP plate connector, studied the influence of the FRP connector layout on the bending stiffness, bearing capacity, and failure mode of specimens; ABAQUS was used to simulate the test. The results showed that different types of arrangements significantly influence the strength and stiffness of the specimen. Naito et al. [16] used 14 different material connectors to conduct three shear performance tests for each connector. The experimental results showed that the rigid truss connector has a higher initial stiffness than the pin connector in the bending mode. Hence, appropriately selecting the different materials and types of connectors and their arrangement can help increase the safety performance of prefabricated sandwich insulation wall panels.

The section form, spacing, insertion angle, and anchorage length of the connector also play important roles in the safety of precast sandwich insulation wall panels. Woltman et al. [17] and Tomlinson et al. [18] studied different types of GFRP connectors in terms of their section diameter, layout spacing, and insertion angle of the joints. The test results showed that the joint length, section diameter, and layout spacing significantly influence the shear strength. The strength and stiffness of the specimen increased with the increase in the embedding angle of the connector. Choi [19] and Ruonan [20] studied the size and shape, anchoring length, section type, and material selection of a single connector. When the anchoring length of the connector was greater than 40 mm, the connector broke. When the anchorage length was sufficient, the shear performance of the connector at an inclination angle of 45° was greater than that at an inclination angle of 30°. Chen [21] and Zhai [22] studied the relationship between the cross-section of FRP connectors and the position of reinforcement distributed in the wall and the connectors. The central cross-sectional shape of the FRP connectors influenced the tensile properties of the FRP connectors. The tensile ductility of FRP connectors with a rectangular cross section was better than that of FRP connectors with a regular cross section. Frankl [23] and Hopkins [24] studied the influence of using connectors, connector arrangement, and concrete layer thickness on the flexural performance of specimens. The long-term deflection of the sandwich insulation board with connectors was found to be better than that of the solid board under long-term loading, and the connector arrangement significantly affected the stiffness of the specimen.

In summary, the safety performance of prefabricated sandwich insulation wall panels has been studied from different aspects based on prefabricated components after curing for 28 days. In practical applications, steam is used in such panels only after 3–5 days of maintenance, and its concrete strength is similar to that of concrete naturally cured for 14 days. There are few studies on whether FRP connectors are safe enough after 14 days of concrete curing. In this work, the shear properties of FRP connectors with different cross-sectional shapes during the curing of precast sandwich thermal-insulation reinforced concrete wall panels for 14 days were studied. Moreover, the ABAQUS finite element analysis software was used for the finite element simulation of the FRP connectors. The shear strength and shear capacity of the connectors as well as the failure mode of the wall panels were compared with the finite element simulation results. Finally, the shear performance of the FRP connectors was parameterized, and the influences of the connector spacing, anchorage depth, and insulation layer thickness on the shear performance of the wall panels were analyzed.

2. Materials and Methods

2.1. Materials

2.1.1. Specimen Mold

The compressive strength test components were poured into cubic 150 mm × 150 mm × 150 mm plastic ABS nondetachable molds. The elastic modulus test member was casted using 300 mm × 150 mm × 150 mm prismatic plastic ABS nonremovable mold. Demolding was conducted after curing to the specified age, as shown in Figure 1b,c.

(**a**) (**b**) (**c**)

Figure 1. Loading instruments and test blocks. (**a**) Test apparatus; (**b**) test cube; (**c**) prism test block.

2.1.2. Loading Instrument

The compressive strength tests were conducted using elastic modulus test loading instruments and hydraulic pressure testing machine (see Figure 1a).

2.1.3. Concrete Compressive Strength Test

The specimens were tested for the compressive strength at different ages using C35 concrete, with three specimens per age, nine in total. Demolding was conducted after 7, 14, and 28 days of maintenance, and the test was conducted after checking for possible problems, as shown in Figure 2. Preloading was set to 1 kN to check whether the instrument worked normally. During the test, the loading speed of the instrument was maintained at 0.6 MPa/s until the specimen was destroyed by adjusting the oil feeding speed, and the data were recorded.

The theoretical compressive strength of C35 concrete used in the compression test was 35 MPa. In the experiment, the measured compressive strength of concrete was 21.7 MPa at 7 days, 26.27 MPa at 14 days, and 35.92 MPa at 28 days (Table 1).

(a) (b)

Figure 2. Compressive strength tests. (**a**) Compressed test block; (**b**) damaged test block.

Table 1. Compressive strength of C35 concrete at different ages.

Curing Age	Test Block Number	Compressive Bearing Capacity (kN)	Compressive Strength (MPa)	Sample Mean (MPa)	Standard Deviation (MPa)	Theoretical Value (MPa)	Error
7 d	Y-KY-7-1	499.73	22.21	21.70	0.56	24.5	11.4%
	Y-KY-7-2	474.75	21.10				
	Y-KY-7-3	489.60	21.76				
14 d	Y-KY-14-1	580.74	25.81	26.27	0.44	28	6.2%
	Y-KY-14-2	592.26	26.32				
	Y-KY-14-3	600.38	26.68				
28 d	Y-KY-28-1	821.25	36.50	35.92	1.46	35	2.6%
	Y-KY-28-2	832.50	37.00				
	Y-KY-28-3	770.85	34.26				

2.1.4. Elastic Modulus Test of Concrete

The specimens were tested for the elastic modulus at different ages using C35 concrete, with three specimens per age, nine in total. They were cured to 7, 14, and 28 days, checked for any possible problems after stripping, and pasted with strain gauges. Finally, the test was started. After the specimen was destroyed, data collection was stopped, as shown in Figure 3.

(a) (b)

Figure 3. Elastic modulus measurement. (**a**) Compressed test block; (**b**) damaged test block.

The theoretical elastic modulus of C35 concrete used in the elastic modulus test was 31,500 MPa. In the experiment, the measured elastic modulus of concrete was 22,115 MPa at 7 days, 25,203 MPa at 14 days, and 32,306 MPa at 28 days (Table 2).

Table 2. Elastic modulus of C35 concrete at different ages.

Curing Age	Test Block Number	Deformation ΔN (με)	Elastic Modulus (MPa)	Sample Mean (MPa)	Standard Deviation (MPa)	Theoretical Value (MPa)	Error
7 d	Y-TX-7-1	3283.95	22,101	22,115	134.55	26,956	17.9%
	Y-TX-7-2	3306.98	22,256				
	Y-TX-7-3	3267.17	21,988				
14 d	Y-TX-14-1	3053.99	25,226	25,203	20.95	29,076	13.32%
	Y-TX-14-2	3050.61	25,198				
	Y-TX-14-3	3049.03	25,185				
28 d	Y-TX-28-1	2801.48	31,986	32,640	589.79	31,500	3.62%
	Y-TX-28-2	2859.72	32,801				
	Y-TX-28-3	2888.58	33,132				

The average yield strength and tensile strength of the steel bars used in the shear test were 413 MPa and 583 MPa, respectively, both exceeding the theoretical value of the HRB400 steel bars. This proves that the performance of the steel bars in the shear test was up to the standard (Table 3).

Table 3. Properties of steel bar materials.

Reinforcement Diameter (mm)	Theoretical Yield Strength (MPa)	Measured Yield Strength (MPa)	Sample Mean (MPa)	Standard Deviation (MPa)	Error	Theoretical Yield Strength (MPa)	Measured Yield Strength (MPa)	Sample Mean (MPa)	Standard Deviation (MPa)	Error
8 mm	400 MPa	420 MPa	413.7	7.77	3.43%	540 MPa	598 MPa	582.7	15.5	7.91%
8 mm	400 MPa	416 MPa				540 MPa	583 MPa			
8 mm	400 MPa	405 MPa				540 MPa	567 MPa			

2.2. Specimen Preparation

In this study, two groups of joints with different section shapes were studied using the bilateral shear method. Thermomass MS30 (L1 connector) was selected as a rectangular cross-sectional connector with a cross-sectional dimension of 5.7 mm × 10 mm, as shown in Figure 4. LJJ-III 116/30-Z was selected as a cross-sectional connector, as shown in Figure 5. Table 4 presents the material parameters of the connectors.

The wall was composed of inner and outer leaf reinforced concrete panels, middle insulation layer, and FRP connectors. Two wall panels with dimensions of 1.2 m × 0.36 m × 0.8 m were prepared in the workshop. The connecting parts were arranged in three rows and two columns, with 6 on each side and symmetrical layout, as shown in Figure 6. The transverse and longitudinal spacings between the connectors was 400 mm, and the spacing between the connectors and the upper and lower ends of the wall was 200 mm. The embedded depth of the connectors at both ends of the concrete was 38 mm. The concrete wall panels on both sides were equipped with a single layer of steel mesh 8 mm in diameter, whereas in the middle they were equipped with a double layer of steel mesh. The protective layer thickness of the steel mesh was 20 mm. The insulation layer was XPS material. When the wall panels were made, the concrete was poured in layers and preserved for 14 days under natural conditions, as shown in Figure 7.

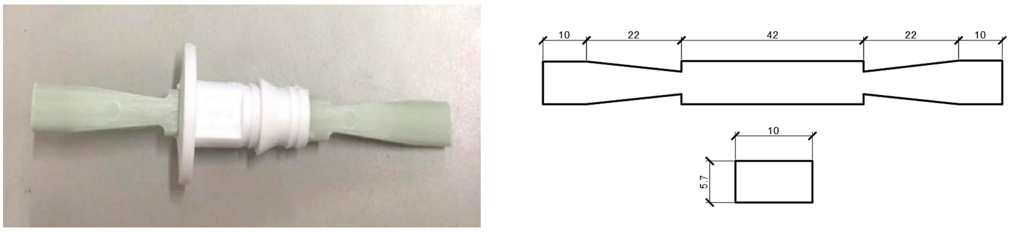

(**a**) (**b**)

Figure 4. L1 connector. (**a**) Real image; (**b**) size details (mm).

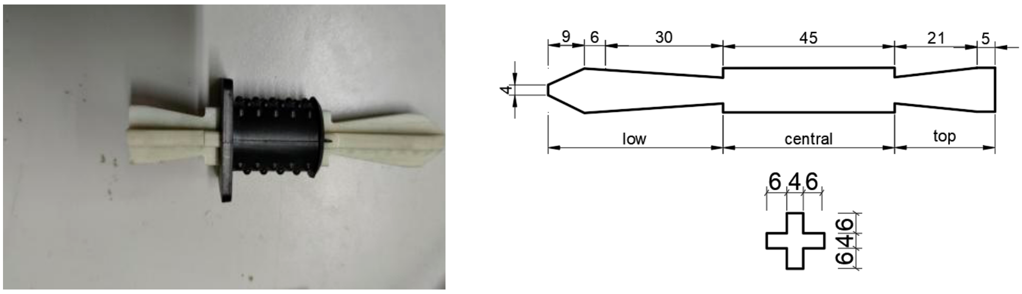

(**a**) (**b**)

Figure 5. L2 connector. (**a**) Real image; (**b**) size detail (mm).

Table 4. Material properties of connectors.

Type of Connector	Tensile Strength/MPa	Tensile Modulus/MPa	Shear Strength/MPa	Bend Strength/MPa	Bending Modulus of Elasticity/GPa
L1 connector	700	4×10^4	57.6	700	3×10^4
L2 connector	890	49.7	59.4	992	44.4

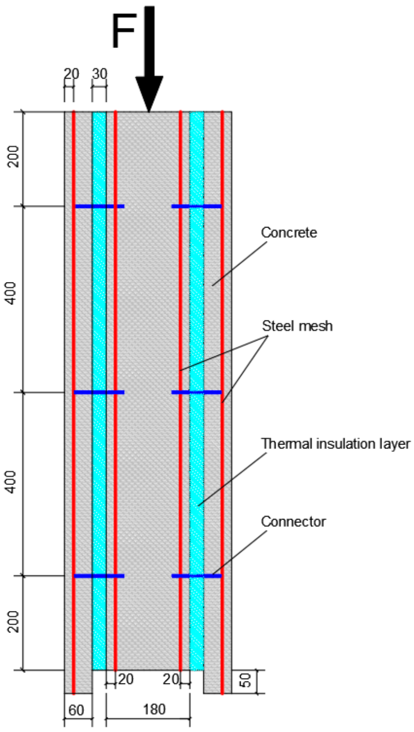

Figure 6. Bilateral shear test (mm).

(a) (b) (c)

Figure 7. Wallboard making process. (**a**) Concrete pouring and vibration; (**b**) insert connector and insulation; (**c**) production completed.

2.3. Load Scheme and Measurement Content

After curing for 14 days under natural conditions, the wall panels were subjected to vertical monotone static loading. The shear strength and shear capacity of the FRP connectors and the failure mode and process of the wall panels were observed during loading. In shear test, bilateral shear was selected, manual hydraulic jack was selected for loading instrument, and a pressure sensor was placed horizontally above the jack to record the applied load in real time. The load was applied by force control. Graded loading was used for the test, with every 5 kN as a level, and the load was held for 5 min at each level, until connector damage or anchorage failure. The pressure sensor above the jack was connected to the DH3818Y static strain tester, and then connected to the computer terminal, which can display the load in real time and record the ultimate bearing capacity. A displacement meter was set up at the left and right ends of the top surface of the intermediate concrete wallboard, which was connected to the static strain tester to measure the absolute displacement of the intermediate concrete wallboard, as shown in Figure 8.

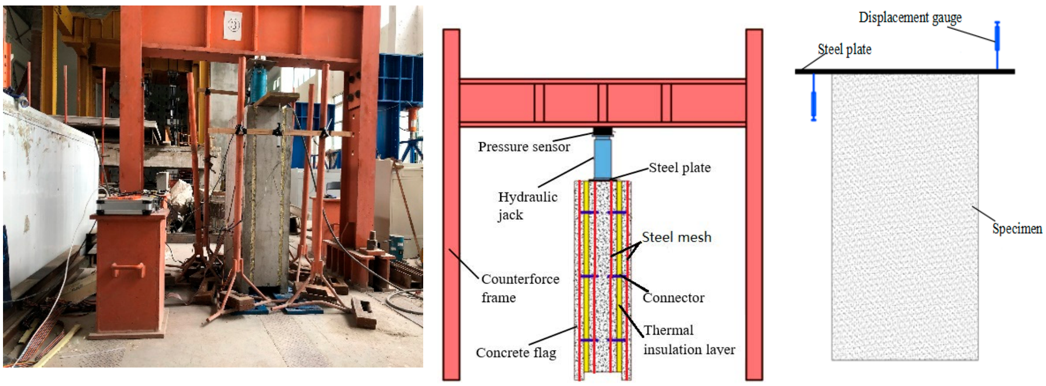

(a) (b) (c)

Figure 8. Schematic of loading device and measuring point. (**a**) Test layout diagram; (**b**) floor plan; (**c**) displacement gauge position diagram.

3. Results and Analysis

3.1. Failure Modes

Two groups of specimens were loaded to observe their failure phenomenon. The failure phenomena of the connectors and concrete were described, and the failure forms of the two groups of specimens were compared and analyzed. The failure process of the wallboard is shown in Figure 9.

The wall panels exhibited three types of failure modes: splitting failure of the fiber layer of the rectangular-section connector in the Q1 wall panel (Figure 10a), fiber fracture in the anchorage of the connector (Figure 10b), and anchoring failure due to concrete damage in anchorage (Figure 10c); these accounted for 25%, 66.7%, and 8.3%, respectively. The three failure modes of the cross-section connector in the Q2 wall panel were as follows:

the splitting failure of the fiber layer of the connector (Figure 11a), the fiber fracture of the anchorage of the connector (Figure 11b), and the anchoring failure due to the concrete damage of the anchorage (Figure 11c); these accounted for 58.3%, 33.3%, and 8.3%, respectively. Therefore, in the shear test of an early-age concrete wall panel with different sections, the failure mode of the wall panel was mainly the failure of the connector material itself. The results showed that the strength of the early-age wall slab concrete met the safety performance requirements of early construction and still had redundancy. Failure morphology of connectors were shown in Table 5.

(**a**) (**b**)

Figure 9. Failure process of wallboard. (**a**) Separation of concrete and insulation; (**b**) final failure result.

(**a**) (**b**) (**c**)

Figure 10. Failure mode of Q1 wallboard connector (part). (**a**) Fiber layer splitting damage; (**b**) fracture at anchorage of connector; (**c**) concrete damage at anchorage.

(**a**) (**b**) (**c**)

Figure 11. Failure mode of Q2 wallboard connector (part). (**a**) Fiber layer splitting damage; (**b**) fracture at the anchorage of connector; (**c**) concrete damage at anchorage.

Table 5. Failure morphology of FRP connectors.

Specimen	Failure Morphology	Proportion
Q1	Fiber layer splitting damage	25%
	Fracture at anchorage of connector	66.7%
	Concrete damage at anchorage	8.3%
Q2	Fiber layer splitting damage	58.3%
	Fracture at anchorage of connector	33.3%
	Concrete damage at anchorage	8.3%

3.2. Load–Displacement Curves

The shear ultimate bearing capacity of the two types of connectors was studied to control the deformation and displacement of the connectors in the shear process. Finally, the load and displacement of the wall panels were plotted, as shown in Figure 12.

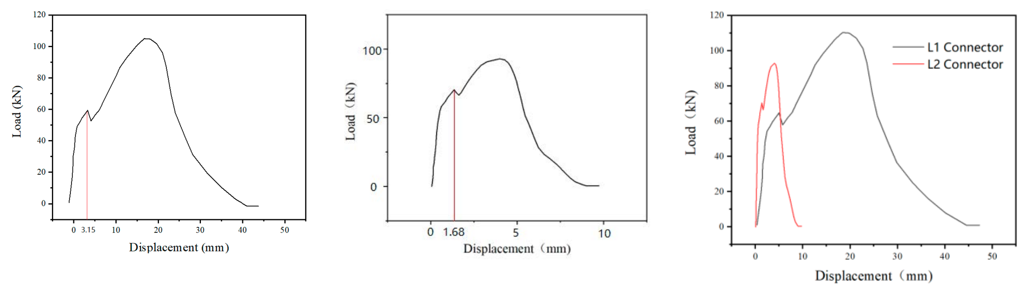

(**a**) (**b**) (**c**)

Figure 12. Load–displacement curve of connector. (**a**) L1 connector; (**b**) L2 connector; (**c**) L1 and L2 connectors.

As shown in the load–displacement curve (Figure 12), the overall trend of load–displacement curves of the two kinds of connectors were similar. The initial load–displacement curves were basically linear. When the displacement of Q1 wall panel and Q2 wall panel was 3.15 mm and 1.68 mm, respectively, the curves show a significant decline and then rise. At this time, it shows that the insulation layer and concrete were basically completely separated, no longer provide bearing capacity, and the shear bearing capacity was all borne by the connectors. When Q1 wall panel displacement reached 18.99 mm, the load reached the ultimate shear bearing capacity of the specimen (100.45 kN), and the ultimate bearing capacity of a single connector was approximately 8.37 kN; when Q2 wall panel displacement reached 5 mm, the load reached the ultimate shear bearing capacity of the specimen (88.687 kN), and the ultimate bearing capacity of a single connector was approximately 7.39 kN. The load dropped sharply, and the wall panels were completely destroyed (Figure 9).

Although the overall trend of load–displacement curves of the two kinds of connectors is similar, their ultimate shear capacity is quite different. The ultimate shear capacity of the L1 connector is 11.793 kN higher than that of the L2 connector. From the load–displacement curve, the displacement of the L1 connector is greater than that of the L2 connector under the same load, indicating that the L1 connector has a better ductility than the L2 connector. Therefore, it provides better safety assurance in actual engineering.

4. Finite Element Analysis

4.1. Shear Simulation of Connectors

4.1.1. Material Constitutive Model

In this simulated concrete constitutive model, the CDP model in ABAQUS was selected. The elastic modulus E of the C35 commercial concrete was 25,203 MPa measured after 14 days, the compressive strength was 26.27 MPa measured after 14 days, and the Poisson's ratio V_c of concrete was 0.2. Table 6 presents the viscosity parameter, dilation angle, and other damage criterion parameters.

Table 6. Failure criterion parameters.

Dilation Angle	Eccentricity	f_{b0}/f_{c0}	K	Viscosity Parameter
30	0.1	1.16	0.6667	0.005

In this simulation, the steel bar was selected to prevent the concrete from cracking in advance; therefore, the double broken line model was selected for the numerical analysis of the constitutive model of the steel bar (Figure 13). The elastic modulus was 2.1×10^5 MPa and Poisson's ratio was 0.3. $E_t = 0.001E_s$.

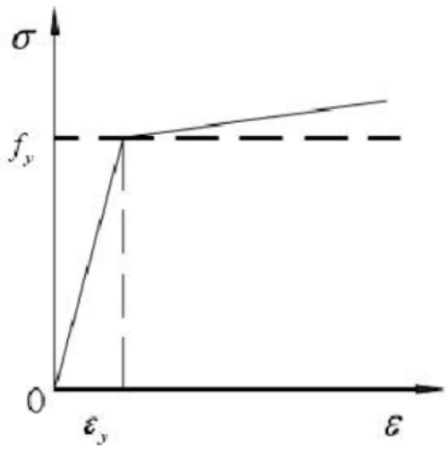

Figure 13. Stress–strain curve of the steel bar.

4.1.2. Establishment of Finite Element Model

In the numerical simulation of the shear strength of composite wall panels, the C3D8R element was selected for the concrete and connectors, and the T3D2 element was selected for the reinforcement. Setting a reference point RP-1 coupled to the upper surface of middle concrete to facilitate loading. Figures 14 and 15 show half the model.

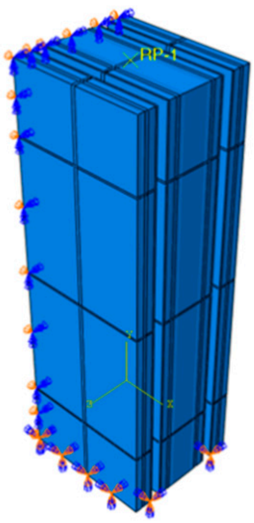

Figure 14. Shear finite element model (side).

Figure 15. Connector model (side).

The dimensions of the finite element model were 1.2 m × 0.36 m × 0.8 m ($h \times W \times L$), and the thicknesses of the three layers of the concrete wall panels from left to right were 6, 18, and 6 cm, respectively. Insulation layer thickness was 30 mm each. Twelve connectors were used in the design of the composite wall panels on both sides, and six were arranged symmetrically on each side.

4.1.3. Finite Element Analysis

Based on the concrete stress cloud shown in Figures 16 and 17, under the ultimate bearing capacity, the shear stress of the two wall panels was the highest at the insertion of the connectors, while the shear stress in the rest of the regions was low. It is proven that the area easily damaged by the wall panel is the anchorage point.

The displacement cloud diagrams of the two types of connectors shown in Figure 18 were analyzed. Because the numerical analysis was to apply displacement load on the middle concrete, the concrete bottom at both ends was completely fixed. It is concluded that the displacement of the connecting piece embedded in the middle concrete is greater than that of the concrete embedded in the outer part.

From the stress cloud diagram of the connector shown in Figure 19, a part of the stress embedded in the concrete at both ends is significantly lower than the shear strength of the connector. The stresses at the anchorage point and the middle segment of the connector stress were the highest and significantly greater than the shear strength of the connector. Combined with the concrete stress and displacement cloud diagram, there are two cases of wall panel failure: concrete cracking failure at the anchorage point leading to anchorage failure, and fiber fracture failure at the anchorage point of the connector.

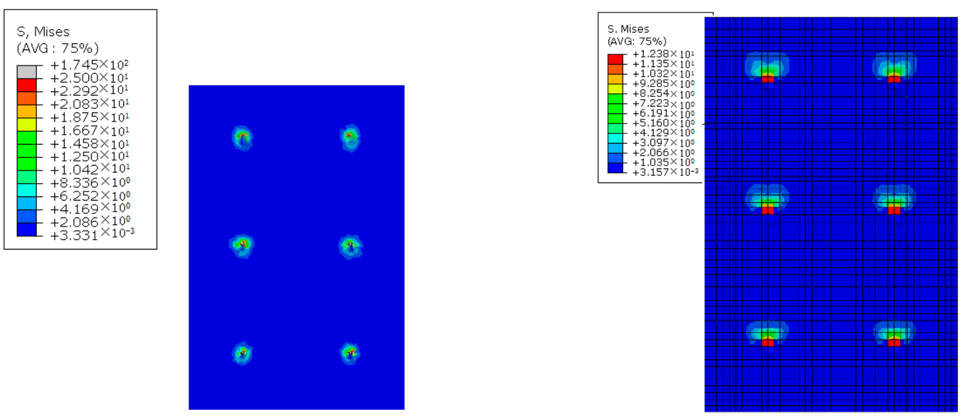

(**a**) (**b**)

Figure 16. Stress cloud diagrams of the concrete in the middle wall panel. (**a**) Q1 wallboard; (**b**) Q2 wallboard.

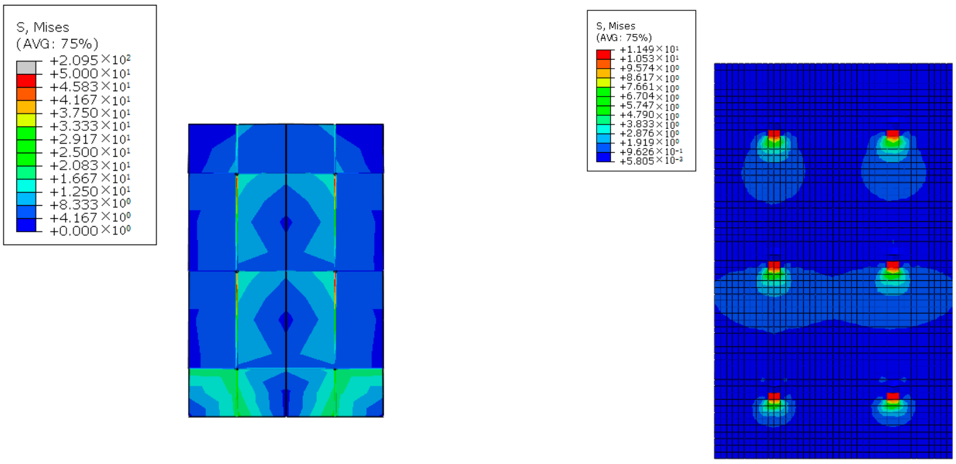

(**a**) (**b**)

Figure 17. Stress cloud diagrams of the concrete on the outer wall panel. (**a**) Q1 wallboard; (**b**) Q2 wallboard.

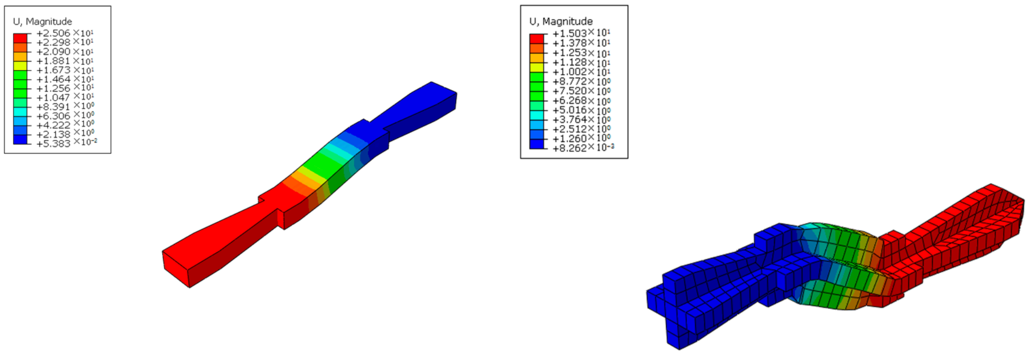

(**a**) (**b**)

Figure 18. Displacement cloud diagrams of connector. (**a**) L1 connector; (**b**) L2 connector.

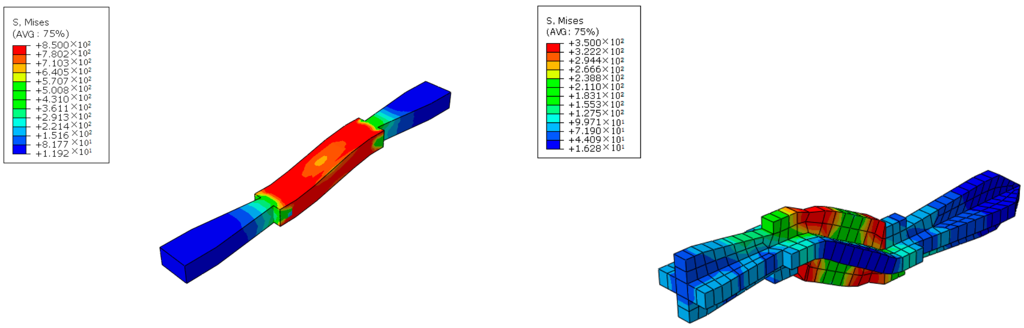

(**a**) (**b**)

Figure 19. Stress cloud diagrams of connector. (**a**) L1 connector; (**b**) L2 connector.

From the load–displacement curve of RP-1 at the coupling point shown in Figure 20, the load and displacement show a linear relationship in the early stage. When the loads of both structures reach approximately 60 kN, the load–displacement curves of the wallboard show a nonlinear growth. Finally, after Q1 reaches 93.972 kN and Q2 reaches 85.625 kN, the image gradually flattens, and the connector is damaged.

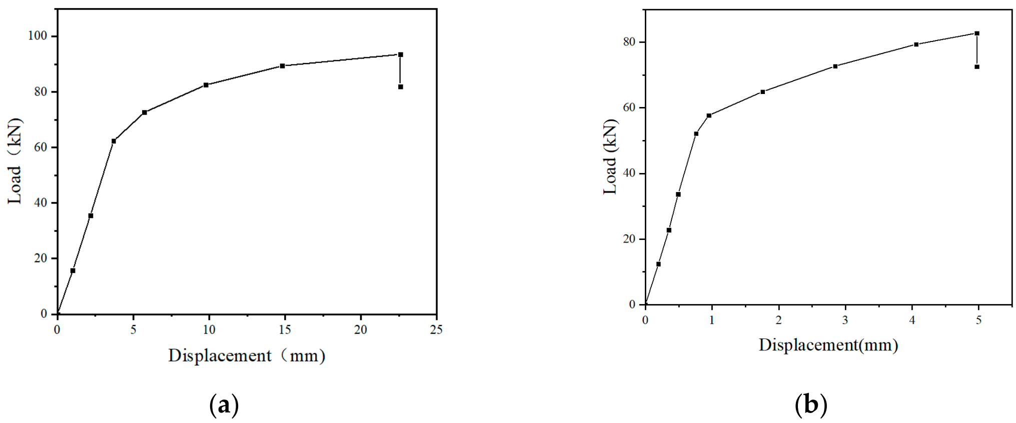

Figure 20. Load–displacement curve of the wall panel. (**a**) Q1 component; (**b**) Q2 component.

The results of the numerical analysis show that the ultimate load of the L1 connector was 46.386 kN, and the ultimate load of bearing capacity was 93.972 kN. The ultimate load of the L2 connector in normal usage was 65.254 kN, and the ultimate load of the bearing capacity was 85.625 kN. Table 7 presents the comparison results. The errors in the simulation and test values of the ultimate load in normal usage and ultimate load of the bearing capacity of the two types of connectors are within the required range. This shows that the established model and selected parameters are reasonable and consistent with the actual situation.

Table 7. Comparison between numerical analysis and experimental results.

Connector Types	Normal Limit Load Simulation Results (kN)	Normal Limit Load Experimentation Results (kN)	Error	Load-Bearing Capacity Limit Load Simulation Results (kN)	Load-Bearing Capacity Limit Load Experimentation Results (kN)	Error
L1	46.386	50.03	7.28%	93.972	100.45	6.45%
L2	65.254	63.64	2.53%	85.625	88.657	3.42%

4.2. Parametric Study on Shear Simulation of Connectors

A numerical analysis of the shear resistance of the wall panels was conducted using ABAQUS, and the reliability of the model was proven through comparative tests. In this section, based on the finite element model and related parameter settings mentioned above, a parametric analysis was conducted on the concrete strength, distance between connecting pieces, arrangement of connecting pieces, and insulation layer thickness when the concrete was cured for 14 days.

4.2.1. Influence of Concrete Strength

To study the influence of the concrete strength grade on the shear capacity of a precast sandwich thermal insulation wall panel after curing for 14 days, based on the above finite element model, a new numerical analysis was conducted by varying only the concrete strength.

Figure 21 shows that the load–displacement curves of concrete with different strength grades coincide. The results indicate that the different strength grades of concrete have little influence on the shear performance of the sandwich wall panel after curing for 14 days.

Table 8 shows the ultimate load in normal usage and ultimate load of the bearing capacity of joints with different concrete strength grades. The normal ultimate load of the wall panel using C30 concrete is 45.53 kN, and that using C60 concrete is 47.60 kN, which is 4.5% higher. The ultimate load of the wall panel using C30 concrete is 94.61 kN, and the maximum ultimate load of the wall panel using C60 concrete is 95.14 kN, which is 0.5% higher. This proves that increasing the strength of the wallboard concrete has little influence on its bearing capacity and can be ignored.

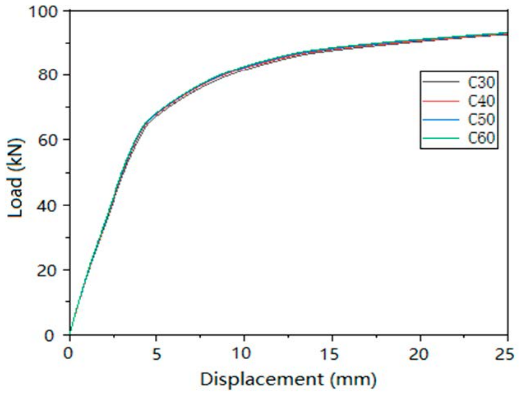

Figure 21. Load–displacement curves of the wallboard under different transverse spacing.

Table 8. Ultimate load of concrete connectors of different strength grades.

Test Block Number	Concrete Strength Grade	Connector Type	Connector Distance (mm)	Insulating Layer Thickness	Normal Limit Load (kN)	Load-Bearing Capacity Limit Load (kN)
QB-30	C30	MS30	400 × 400	30	45.53	94.61
QB-40	C40	MS30	400 × 400	30	46.19	94.83
QB-50	C50	MS30	400 × 400	30	46.99	95.01
QB-60	C60	MS30	400 × 400	30	47.60	95.14

4.2.2. Influence of Connector Spacing

To consider the influence of the spacing of connecting pieces on the wall panel after 14 days of concrete curing, the other parameters were kept unchanged on the basis of the above shear numerical analysis, and the transverse and longitudinal spacings between the connecting pieces were changed to conduct a new numerical analysis. Table 9 presents the spacing of the connectors. The dimensions of the wall panel were 2360 mm × 1580 mm × 360 mm, no holes, and the insulation layer thickness was 30 mm. The prefabricated sandwich wall panel with MS30 (L1) connector was used for the analysis.

Table 9. Wallboard loads under different transverse and longitudinal spacings.

Wallboard Number	Connector Type	Connector Spacing (mm)	Usage Amount	Normal Service Load of Wall Panel (kN)	Normal Service Load of Single Connector (kN)
QB1	MS30	250 × 400	72	206.05	2.86
QB2	MS30	300 × 400	60	177.03	2.95
QB3	MS30	400 × 400	48	154.08	3.21
QB4	MS30	500 × 400	36	101.22	2.81
QB5	MS30	600 × 400	36	104.25	2.89
QB6	MS30	400 × 250	72	202.89	2.82
QB7	MS30	400 × 300	64	190.46	2.98
QB8	MS30	400 × 500	40	113.10	2.83
QB9	MS30	400 × 600	32	99.67	3.11

Based on the load–displacement curves (QB1–QB5) of the wallboard under different transverse spacing shown in Figure 22, it can be concluded that different transverse spacing has a significant influence on the shear performance of the wallboard. The normal ultimate loads of QB1–QB5 were 206.05, 177.03, 154.08, 101.22, and 104.25 kN. The QB1 wall panel uses 72 connectors, and the transverse spacing of the connectors is the smallest, whereas the QB5 wall panel uses 36 connectors, and the transverse spacing of the connectors is the highest. This shows that the transverse spacing between the connectors increases by 2.4 times, the number of connectors decreases by 50%, and the ultimate load in normal usage decreases by 49.45%.

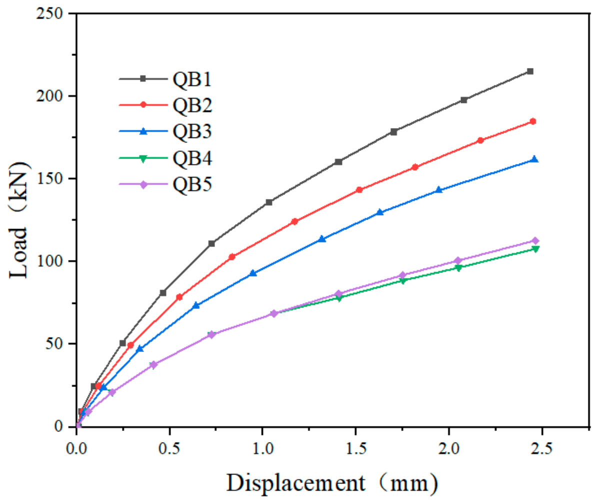

Figure 22. Load–displacement curves of the wallboard with different transverse spacings.

As shown in Table 9, the distance between the QB1 and QB2 connectors increases by 1.2 times, and the number of connectors in usage decreases by 16.67%. It can be concluded that the ultimate load in normal service is reduced by 14.08% and the load of the single connector is increased by 3.15%. From QB2 to QB3, the distance between the connectors is increased by 1.3 times, and the number of connectors is reduced by 20%. It can be concluded that the ultimate load in normal service is reduced by 12.96%, and the load of the single connector is increased by 8.81%. From QB3 to QB4, the distance between the connectors increases by 1.25 times, and the number of connectors decreases by 25%. It can be concluded that the ultimate load in normal service is reduced by 34.30%, and the load of the single connector is reduced by 12.46%. From QB4 to QB5, the connecting piece spacing increases by 1.2 times, and the number of connectors in usage remains unchanged. The ultimate load in normal usage increases by 3.00%, and the load of the single connector increases by 2.85%. Therefore, the greater the transverse spacing between the FRP connectors, the lower the normal service acting on the wall panels. When the transverse spacing increases from 400 mm to 500 mm, the load of the wall panels and connectors decreases most evidently. When the transverse spacing is 400 mm, the single connector can bear the maximum load.

From the load–displacement curves (QB3, QB6–QB9) of the connectors at different longitudinal distances shown in Figure 23, it can be concluded that the longitudinal distance significantly influences the shear performance of the wall panels. The ultimate loads of the five wall panels in normal usage are 202.89, 190.46, 154.08, 113.10, and 99.67 kN. The QB6 wall panel uses 72 connectors, and the transverse spacing between the connectors is the smallest, whereas the QB9 wall panel uses 32 connectors, and the transverse spacing between the connectors was the largest. It shows that the transverse spacing of connectors increases by 2.4 times, the number of connectors decreases by 55.6%, and the ultimate load in normal use decreases by 50.87%.

As shown in Table 9, the distance between QB6 and QB7 connectors increases by 1.2 times, and the number of connectors in usage decreases by 11.11%. It can be concluded that the ultimate load in normal service is reduced by 6.13%, and the load of the single connector is increased by 5.67%. From QB7 to QB3, the distance between the connectors is increased by 1.3 times, and the number of connectors is reduced by 20%. It can be concluded that the ultimate load of the normal service is reduced by 19.10%, and the load of the single connector is increased by 7.72%. From QB3 to QB8, the distance between the connectors increases by 1.25 times, and the number of connectors decreases by 16.67%. It can be concluded that the ultimate load in normal service is reduced by 26.60%, and the load of the single connector is reduced by 13.43%. From QB8 to QB9, the distance between connectors is increased by 1.2 times, and the number of connectors is reduced by 16%. It can be concluded that the ultimate load in normal service is reduced by 11.87%, and the load of single connector is increased by 9.00%. Therefore, the greater the longitudinal spacing between the FRP connectors, the lower the normal service limit load of the wall panels. When the longitudinal spacing increases from 400 mm to 500 mm, the load of the wall panels and connectors decreases most evidently. A single connector can bear the maximum load when the longitudinal spacing is 400 mm.

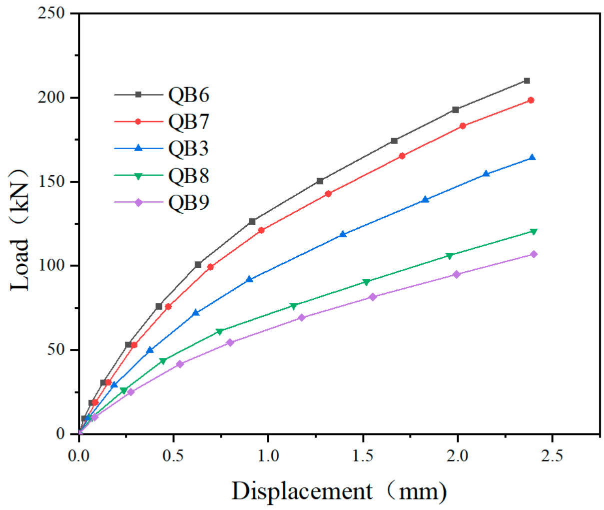

Figure 23. Load–displacement curves of the wallboard under different longitudinal spacings.

4.2.3. Influence of Anchorage Depth of Connector

To consider the influence of the anchorage depth of the connector on the wall panel, the anchorage depth of the connector was changed to 51 mm for the numerical analysis based on the numerical analysis of the shear.

As shown in the load–displacement curve (Figure 24) of the wallboard with an anchorage depth of 51 mm, the normal service load of the wallboard at this time is 58.641 kN. Figure 20 shows that the normal service load of the wall panel is 45.386 kN when the anchorage depth is 38 mm. By comparison, the anchorage depth increases by 34.21%, and the shear capacity of the wall panel increases by 29.21%. Therefore, the anchorage depth significantly influences the shear performance of the connection.

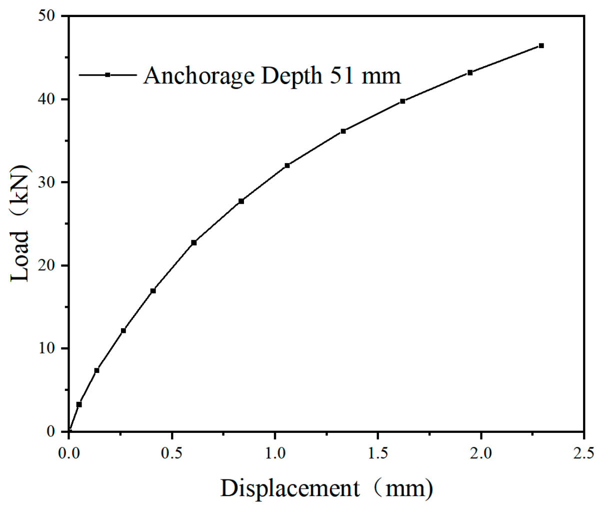

Figure 24. Load–displacement curve of wall panel with an anchorage depth of 51 mm of the connector.

4.2.4. Influence of Insulation Layer Thickness

To study the effect of thermal insulation layer thickness on the shear performance of FRP connectors, in this part, insulation layers with thicknesses of 30, 40, and 50 mm were selected for the finite element simulation under the premise that the other simulation parameters remain unchanged. Figure 25 shows the load–displacement curve obtained by the numerical simulation.

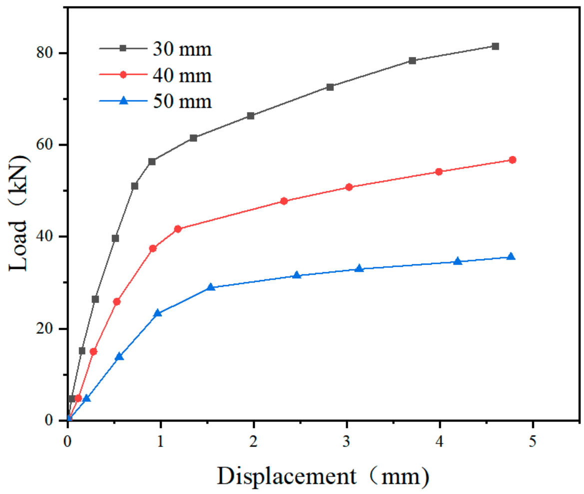

Figure 25. Load–displacement curves of FRP connectors with different insulation thicknesses.

The comparison between Table 10 and load–displacement curves showed that the insulation layer thickness significantly affects the shear performance of GFRP connectors. When the ultimate load in normal usage is reached, the corresponding load increases by 51.48% when using the 40 mm-thick insulation layer compared with using the 50 mm-thick insulation layer, and the corresponding load increases by 44.00% when using the 30 mm-thick insulation layer compared with using the 40 mm-thick insulation layer. The results showed that the shear performance of FRP connectors can be effectively enhanced by reducing the insulation layer thickness on the premise of satisfying the thermal insulation effect.

Table 10. Ultimate load under different insulation thicknesses.

Insulating Layer Thickness	30 mm	40 mm	50 mm
Normal limit load value (kN)	70.513	48.967	32.326
Ultimate load value of bearing capacity (kN)	85.315	65.915	43.818

5. Conclusions

Through tests and simulations using the finite element analysis software ABABQUS, the mechanical properties of two types of FRP connectors anchored in concrete for 14 days of curing were analyzed. The following conclusions can be drawn from the results:

(1) In the shear test of the wall panel cured in concrete for 14 days, the sandwich insulation composite wall panel exhibited three types of failure modes: fiber layer splitting failure of the connector, fiber fracture at the anchorage of the connector, and concrete failure at the anchorage of the connector. The material of the connector itself was mainly damaged, and the concrete strength was redundant.

(2) The failure mode of the specimen was the cut off of the connector. The average ultimate shear bearing capacity of a single rectangular-section connector (L1) was 8.37 kN and that of a single cross-sectional connector (L2) was 7.39 kN. The connector exhibited better shear resistance, and the L1 connector had better ductility than the L2 connector. Based on the standard calculation results [25], the two types of connectors meet the actual engineering safety requirements and have large safety reserves.

(3) The results of the numerical analysis were close to the test results, and the error was less than 10%. This shows that the established model and selected parameters are reasonable and consistent with the actual situation.
(4) When the curing age of concrete was 14 days, a shear parameterization study of the wall panel showed that the influence of the concrete strength grade on the bearing capacity of the composite wall panel can be ignored. The spacing between the connecting pieces had a significant influence on the bearing capacity of the wall panels. The spacing between the connecting pieces was inversely proportional to the ultimate load of the wall panel in normal usage. When the transverse spacing (longitudinal spacing) was increased from 400 mm to 500 mm, the ultimate load decreased the most. The anchorage depth of the connectors increased by 34.21%, and the shear capacity of the wall panels increased by 29.21%. These results showed that the anchorage depth significantly influences the shear capacity of the connector. An analysis of the thermal insulation layer showed that, the thicker the thermal insulation layer, the lower the shear capacity of the specimen.

Author Contributions: Conceptualization, D.C., B.C. and Z.Y.; methodology, D.C., B.C. and Z.Y.; software, K.L. and Z.Y.; formal analysis, B.C., D.C. and K.L.; writing—original draft preparation, K.L. and Z.Y.; writing—review and editing, D.C., B.C. and X.K. All authors have read and agreed to the published version of the manuscript.

Funding: This work was supported by Mechanical Properties Research of FRP Connectors in Fabricated Concrete Sandwich Insulation Wall Panels after Fire (KJ2021A0608), Natural Science Foundation of Anhui Province (19080885ME173), Research and Development project of China State Construction International Holdings Limited (CSCI-2020-Z-06-04), Science and Technology Project of Anhui Province Housing and Urban–Rural Construction (2020-YF47), and Science and Technology R&D Project of China Construction Corporation (CSCEC-2019-Z-4).

Institutional Review Board Statement: No ethical approval was required for this study.

Informed Consent Statement: The study did not involve humans.

Data Availability Statement: The data presented in this study are available on request from the corresponding author.

Acknowledgments: The authors gratefully acknowledge the financial support provided by Anhui Province Housing Urban and Rural Construction Science and Technology Project (2020-YF47).

Conflicts of Interest: The authors declare no conflict of interest.

References

1. Liu, K.; Wang, X.; Xue, J.; Shen, L.; Jin, S. Research on comparison of development status of domestic and foreign prefabricated buildings and countermeasures. *Ind. Constr.* **2021**, *53*, 19–24. [CrossRef]
2. Chen, D.; Deng, J.; Cheng, B.; Wang, Q.; Zhao, B. New Anticracking Glass-Fiber-Reinforced Cement Material and Integrated Composite Technology with Lightweight Concrete Panels. *Adv. Civ. Eng.* **2021**, *2021*, 7447066. [CrossRef]
3. Chen, D.; Li, P.; Cheng, B.; Chen, H.; Wang, Q.; Zhao, B. Crack Resistance of Insulated GRC-PC Integrated Composite Wall Panels under Different Environments: An Experimental Study. *Crystals* **2021**, *11*, 775. [CrossRef]
4. Bai, Z.X.; Gao, J.W.; Liu, X.C.; Zhang, D.J.; Deng, Y.P.; Qiang, S.; Bai, Y.T. Research on the connection performance of glassfiber reinforced plastics connector of sandwich wall. *Ind. Constr.* **2020**, *50*, 169–176. [CrossRef]
5. Wei, Y.; Zhang, Y.; Chai, J.; Wu, G.; Dong, Z. Experimental investigation of rectangular concrete-filled fiber reinforced polymer (FRP)-steel composite tube columns for various corner radii. *Compos. Struct.* **2020**, *244*, 112311. [CrossRef]
6. Wei, Y.; Zhu, C.; Miao, K.; Zheng, K.; Tang, Y. Compressive performance of concrete-filled steel tube columns with in-built seawater and sea sand concrete-filled FRP tubes. *Constr. Build. Mater.* **2021**, *317*, 125933. [CrossRef]
7. Wei, Y.; Bai, J.; Zhang, Y.; Miao, K.; Zheng, K. Compressive performance of high-strength seawater and sea sand concrete-filled circular FRP-steel composite tube columns. *Eng. Struct.* **2021**, *240*, 112357. [CrossRef]
8. He, Z.F. Strength Loss and Prevention of Concrete Members after Steam Curing. *Concrete* **1993**, *5*, 53–56.
9. Su, Y.; Xu, Z.H.; Chou, J.N.; Kang, Z.J. Effect of Steam Curing System on Early Strength of Precast Concrete Impact study. *China Concr. Cem. Prod.* **2019**, 48–50. [CrossRef]
10. Salmon, D.C.; Einea, A.; Tadros, M.K.; Culp, T.D. Full Scale Testing of Precast Concrete Sandwich Panels. *Struct. J.* **1997**, *94*, 354–362.

11. Salmon, D.C.; Einea, A. Partially Composite Sandwich Panel Deflections. *J. Struct. Eng.* **1995**, *121*, 778–783. [CrossRef]
12. Kazem, H.; Bunn, W.G.; Seliem, H.M.; Rizkalla, S.H.; Gleich, H. Durability and long term behavior of FRP/foam shear transfer mechanism for concrete sandwich panels. *Constr. Build. Mater.* **2015**, *98*, 722–734. [CrossRef]
13. Ekenel, M. Testing and Acceptance Criteria for Fiber-Reinforced Composite Grid Connectors Used in Concrete Sandwich Panels. *J. Mater. Civ. Eng.* **2014**, *26*, 06014004.1–06014004.5. [CrossRef]
14. Portal, N.W.; Thrane, L.N.; Lundgren, K. Flexural behaviour of textile reinforced concrete composites: Experimental and numerical evaluation. *Mater. Struct.* **2016**, *50*, 4. [CrossRef]
15. Chen, A.; Norris, T.G.; Hopkins, P.M.; Yossef, M. Experimental investigation and finite element analysis of flexural behavior of insulated concrete sandwich panels with FRP plate shear connectors. *Eng. Struct.* **2015**, *98*, 95–108. [CrossRef]
16. Naito, C.; Hoemann, J.; Beacraft, M.; Bewick, B. Performance and Characterization of Shear Ties for Use in Insulated Precast Concrete Sandwich Wall Panels. *J. Struct. Eng.* **2012**, *138*, 52–61. [CrossRef]
17. Woltman, G.; Tomlinson, D.; Fam, A. Investigation of Various GFRP Shear Connectors for Insulated Precast Concrete Sandwich Wall Panels. *J. Compos. Constr.* **2013**, *17*, 711–721. [CrossRef]
18. Tomlinson, D.G.; Teixeira, N.; Fam, A. New Shear Connector Design for Insulated Concrete Sandwich Panels Using Basalt Fiber-Reinforced Polymer Bars. *J. Compos. Constr.* **2016**, *20*, 04016003. [CrossRef]
19. Choi, K.-B.; Choi, W.-C.; Feo, L.; Jang, S.-J.; Yun, H.-D. In-plane shear behavior of insulated precast concrete sandwich panels reinforced with corrugated GFRP shear connectors. *Compos. Part B Eng.* **2015**, *79*, 419–429. [CrossRef]
20. Liu, R.N. Research on Design of Connector for Precast Concrete Sandwich Panel Based on Strength Theory. Ph.D. Thesis, Wuhan University of Technology, Wuhan, China, 2015.
21. Chen, C.; Zhang, Z.; Ding, L.; Lei, F.; Chen, D. Experimental Research on Tensile Properties of Prefabricated Sandwich Insulation Wallboard FRP Connector. *Ind. Constr.* **2019**, *49*, 58–63. [CrossRef]
22. Zhai, X.M.; Wang, X.M. Experimental study on mechanical performance of composite connector for prefabricated concrete sandwich panels. *Build. Struct.* **2015**, *48*, 73–78. [CrossRef]
23. Frankl, B.A.; Lucier, G.W.; Hassan, T.K.; Rizkalla, S.H. Behavior of precast, prestressed concrete sandwich wall panels reinforced with CFRP shear grid. *PCI J.* **2011**, *52*, 42–54. [CrossRef]
24. Hopkins, P.M.; Norris, T.; Chen, A. Creep behavior of insulated concrete sandwich panels with fiber-reinforced polymer shear connectors. *Compos. Struct.* **2017**, *172*, 137–146. [CrossRef]
25. *JG/T 561*; Xue, W.; Qin, H.; Liu, Y.; Li, X.; Hu, X.; Zhu, Y.; Liu, G.; Li, Y.; Wang, X.; Miao, D.; et al. Frber-Reinforced Polymer Connector for Precast Sandwich Insulation Walls. Ministry of Housing and Urban-Rural Development: Beijing, China, 2019.